JAERI-M
88-103

ACCURACY EVALUATION OF THE CURRENT DATA AND METHOD APPLIED TO SHIELDING DESIGN OF THE FUSION EXPERIMENTAL REACTOR (FER)

June 1988

Seiji MORI*, Takeshi KOBAYASHI and Yasushi SEKI

日本原子力研究所
Japan Atomic Energy Research Institute

JAERI-Mレポートは，日本原子力研究所が不定期に公刊している研究報告書です。
入手の問合わせは，日本原子力研究所技術情報部情報資料課（〒319-11茨城県那珂郡東海村）あて，お申しこしください。なお，このほかに財団法人原子力弘済会資料センター（〒319-11 茨城県那珂郡東海村日本原子力研究所内）で複写による実費頒布をおこなっております。

JAERI-M reports are issued irregularly.
Inquiries about availability of the reports should be addressed to Information Division Department of Technical Information, Japan Atomic Energy Research Institute, Tokai-mura, Naka-gun, Ibaraki-ken 319-11, Japan.

編集兼発行　日本原子力研究所
印　　刷　㈱高野高速印刷

Accuracy Evaluation of the Current Data and Method Applied to Shielding Design of the Fusion Experimental Reactor (FER)

Seiji MORI*, Takeshi KOBAYASHI and Yasushi SEKI

Fusion Experimental Reactor Team
Naka Fusion Research Establishment
Japan Atomic Energy Research Institute
Naka-machi, Naka-gun, Ibaraki-ken

(Received May 13, 1988)

Shielding benchmarking study of the current data and method applied to the Fusion Experimental Reactor (FER) was performed. First, neutron and gamma ray fluxes were calculated by the one-dimensional S_N code using various cross section libraries and the continuous energy Monte Carlo code. The results were compared in terms of the S_N/MC ratio. The worst ratios are about 0.5 and 0.25 for neutron flux and gamma ray flux, respectively. Next, the analytical calculations of the iron sphere transmission experiment of 14 MeV neutrons were performed to examine the accuracy of cross section data of iron, which is the most important material of shield. The E/C ratio is larger than 2 even if the continuous energy Monte Carlo code was used. Thirdly, the influence of geometrical representation of the shield was investigated by comparing the homogeneous model and the heterogeneous model (alternating layers of SS316 and water). As a result, it was made clear that the homogeneous model underestimates neutron flux by a factor of 2. Finally, the necessity of benchmark experiment and improvement of cross section library was pointed out as the further R&D issues.

Keywords: Accuracy, Shielding Design, Fusion Experimental Reactor, Nuclear Data, Kerma Factor, Discrete Ordinate, Monte Carlo, Benchmark Calculation, Nuclear Heat Deposition, Hetrogeneity

---

* On leave from Kawasaki Heavy Industries, Ltd.

JAERI－M 88－103

核融合実験炉（ＦＥＲ）の遮蔽設計に適用されるデータおよび計算手法の精度評価

日本原子力研究所那珂研究所核融合実験炉特別チーム
森　清治*・小林　武司・関　泰

（１９８８年５月１３日受理）

核融合実験炉（ＦＥＲ）の遮蔽設計に用いる核データおよび計算手法による中性子束およびガンマ線束計算値の精度を評価した。各種群定数ライブラリーを用いた１次元 S_N 計算と連続エネルギーモンテカルロ計算を実施し，その比較結果を両者の比率（S_N／MC比）の形で整理した。その結果，最悪の場合，中性子束では0.5，ガンマ線束では0.２５程度の値となった。次に遮蔽体材料として最も重要な鉄について１４MeV中性子の透過実験の解析を行ない，測定値との比較を行なった。最良の計算値でもE／C比は２以上の大きな値となっている。最後に遮蔽体のモデル化（均質モデルと非均質モデル）の影響を検討した結果，ＳＳ３１６と水の多重層（非均質モデル）とした場合に比べ均質モデルはファクター２程度まで危険側の結果を与えることが判明した。今回の検討から今後の課題としてベンチマーク実験と核定数ライブラリーの改善の必要性を指摘した。

那珂研究所：〒311－01　茨城県那珂郡那珂町大字向山８０１－１
＊　外来研究員　　川崎重工（株）

Contents

目　　次

1. Introduction

Optimization (minimization) of shield configuration (shield thickness) especially at the torus inboard region has been required in the course of the design for the Fusion Experimental Reactor (FER) because the shield thickness has a large impact on the reactor size and the cost[1),(2)]. It is necessary, therefore, to evaluate calculation errors caused by the current methods and data used in the shielding design in order to validate the optimization study. Various causes which generate calculation errors in shielding design process are illustrated in Fig. 1.1. Error analyses must be carried out systematically to clear effect of each cause on calculation accuracy separately. Alsmiller et.al. discussed the uncertainty of the shielding reponses of toroidal field coil due to the cross section uncertainties[(3)], and Furuta et.al. discussed the accuracy of the multi-group transport calculation[(4)]. In the design of FER, accuracy of the shielding calculation has been discussed from the viewpoints of the geometrical representation and the multi-group transport calculation[(5),(6)].

This study includes three major items (benchmark calculations); 1) uncertainty due to multi-group approximation, 2) uncertainty due to cross section data, 3) uncertainty due to geometrical representation. In the first benchmark calculation accuracy of the discrete ordinates (S_N) transport calculation using multi-group constants was discussed by comparing the results with those by the continuous energy Monte Carlo calculation. Influences of using different nuclear data files and differently processed data libraries on the calculated results were also investigated in this study.

In the second benchmark calculations, the selected benchmark experiments with iron sphere using 14 MeV neutron source were analyzed with the current methods and data, and calculated results were compared with the measured values.

In the third benchmark calculation, influence of heterogeneous representation of the shield structure was investigated. Two kinds of the one-dimensional model were analyzed; one is the homogeneous mixture of structural material and water, another is the alternating layers of structure material and water.

The conclusions of the study will be used to provide predicted shielding properties with design margin (or safety factor) when the current methods and data are applied to the shield design.

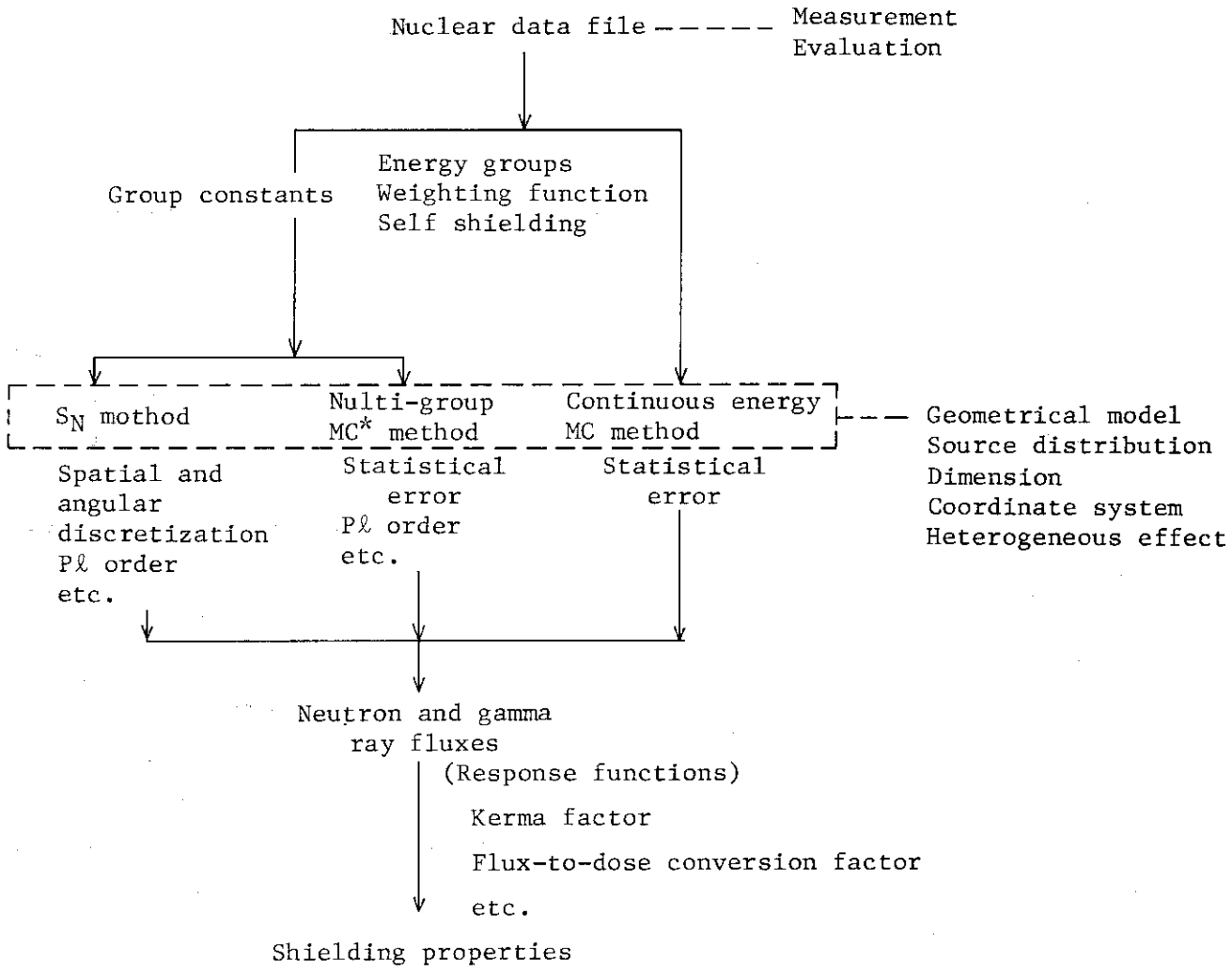

Fig. 1.1 Causes of Calculation Errors in Shielding Design

2. Accuracy Evaluation of Multi-Group S_N Calculation

2.1 Calculation method

The multi-group transport calculations were performed by using the one-dimensional discrete ordinates code ANISN[7] which is used most frequently in the design of FER. The calculation used an S_8 symmetric angular quadrature set and a P_5 Legendre expansion (P_3 for VITAMIN-C) for the scattering cross section. Main features of the several cross section libraries used in the S_N calculations are summarized in Table 2.1[8]-[14]. All the libraries except the FSXJ3T1[12] based on the JENDL-3T library[13]* are neutron and gamma ray coupled sets. All the neutron cross sections are for infinite dilution. The GICX40[8] is used most often at present for fusion reactor design widely in Japan, and the GICXFNS[11] is used for analytical study of 14 MeV neutron experiments at FNS(the fusion neutronics source at JAERI). The GICX40V4[8] and the GICX50[10], however, have not been used often so far and propriety of their application has not been assured yet. Another 171 neutron, 36 gamma ray group cross section library was generated from the DLC41/VITAMIN-C library[14].

The infinite cylindrical model as shown in Fig. 2.1 was used in the first benchmark calculation. Atomic densities of the materials are shown in Table 2.2.

The continuous energy Monte Carlo calculation by the MCNP code[15] was performed. The point-wise cross sections used in MCNP are based on the ENDF/B-IV data file[9]. The same geometrical model as the one-dimensional S_N calculation was used in the Monte Carlo calculations. In this case, however, a pair of reflecting surfaces were assumed for the base planes of the cylinder. Track length estimators and surface crossing estimators were employed to calculate the shielding responses.

An isotropic and uniformly distributed 14.1 MeV monoenergetic neutron source was assumed in the plasma region. In the multi-group calculations, however, neutron source energy ranges 15-13.72 MeV for GICX40, GICX40V4 and GICX50; 14.218-13.967 MeV for GICXFNS; 14.10-13.88 MeV for FSXJ3T1; 14.19-13.84 MeV for VITAMIN-C.

---

* JENDL-3T is a temporary file for testing the evaluated data of JENDL-3. The data in JENDL-3T will be partly revised in JENDL-3.

2.2 Calculation results

2.2.1 SS316/water shield

(1) Neutron and gamma ray flux

Neutron fluxes and gamma ray fluxes are compared in Fig. 2.2 to Fig. 2.5 and Table 2.3 between the multi-group S_N calculations and the continuous energy Monte Carlo calculations in terms of ANISN to MCNP ratio (S_N/MC ratio). Neutron fluxes calculated by ANISN are smaller than those by MCNP. Discrepancies between ANISN and MCNP results increase with depth into the shield. The S_N/MC ratios seem to increase at the outer surface of the shield. This is because the flux calculated by ANISN is given at the midpoint of the interval (i.e. 0.5 cm from the surface). Although the discrepancies partly originate from the difference in nuclear data fliles in the case of GICX40 and FSXJ3T1, they are mainly due to the multi-group approximation, e.g., the window effect of the resonance cross section minima, when the same nuclear data file (ENDF/B-IV) as MCNP are used. The worst S_N/MC ratios in the total neutron fluxes are about 0.5 for GICX40 and around 0.7 for GICXFNS, GICX40V4, GICX50, FSXJ3T1 and VITAMIN-C.

The gamma ray flux calculated using GICX40 is much smaller than that of MCNP. The worst S_N/MC ratio is around 0.25. While, the gamma ray flux calculated using GICXFNS, GICX40V4, and GICX50 are much larger than that of MCNP. The worst ratio is around 2. Large difference is observed over all the thickness, even in the first wall region. The gamma ray flux calculated with VITAMIN-C shows much better agreement with that of MCNP, and the worst ratio is about 0.76.

The S_N/MC ratios in neutron and gamma ray fluxes at the position 60 cm from the first wall are summarized in Table 2.3. Accuracy of neutron fluxes seem to be improved by using the libraries based on the ENDF/B-IV and JENDL-3T files instead of the ENDF/B-III file. While, the secondary gamma ray fluxes show large disagreement between these results. Only VITAMIN-C gives the reasonable values.

The secondary gamma ray production cross sections were used in the S_N calculation and the Monte Carlo calculation. Insufficiencies in the production data, therefore, affect the accuracy of the calculation of the gamma ray flux. As stated in the next section, the accuracy of the secondary gamma ray flux was evaluated by the integral energy balance method[16], which is not affected by the insufficiency in the production data, in terms of the total energy deposition.

(2) Nuclear heat deposition

The S_N/MC ratios of the nuclear heat deposition by neutron and gamma ray are shown in Fig. 2.6 and Fig. 2.7, respectively. The ANISN calculation using GICX40 underestimates both neutron and gamma ray heating. Discrepancies in neutron heating are relatively small and the worst ratio is about 0.77. Discrepancies in gamma ray heating are rather large and the worst ratio is about 0.36. This tendency is the same as that of neutron and gamma ray fluxes mentioned above.

In order to check the accuracy of the calculation of nuclear heating, we have also calculated total heat deposition in the shield using the integral energy balance method. The total nuclear heat deposition in the shield, H_t can be calculated by the following equation;

$$H_t = H_{in} + \Sigma R_{ij}Q_{ij} + \Sigma R_{ij}E_{ij} - L_nE - L_gE \qquad (1)$$

where,

E_{in}: Neutron energy incident on the first wall from plasma, 14.1 MeV
R_{ij}: Reaction rate in shield for reaction i of element j
Q_{ij}: Q value for reaction i of element j
E_{ij}: Energy deposited per reaction i in element j from radioactive decay of the residual nucleus
L_nE: Net neutron energy transported out of shield
L_gE: Net gamma ray energy transported out of shield

Here, neglecting the third, fourth and fifth terms because these are much smaller than the other terms, the equation (1) becomes;

$$H_t = E_{in} + \Sigma R_{ij}Q_{ij} \qquad (2)$$

Table 2.4 shows the results of neutron, gamma ray and total nuclear heat deposition per one DT neutron calculated by the different methods and data. From these results, the following observations can be drawn;

1) Results of the neutron heating do not differ much between the differnt methods and data.
2) Results of the gamma ray heating show large disagreement between the results. Results of GICX40 is smaller than those of MCNP and the integral energy balance method.
3) Total heating calculated using the libralies generated by the NJOY code based on the ENDF/B-IV file is $\gtrsim$ 30 MeV per one DT neutron

and this is clearly too high.

4) The result calculated by the integral energy balance method agrees well with the those of MCNP using the ENDF/B-IV file.

(3) Neutron energy spectrum

Neutron energy spectra at the position 50 cm from the first wall calculated by ANISN and MCNP are compared in Fig. 2.8. In the energy range of several MeV, results by ANISN/GICX40 is much smaller than the other results. This is attributed to the difference of iron cross sections between ENDF/B-III and ENDF/B-IV as shown in the next chapter. Large variation of the magnitude of the group flux around 5 MeV by MCNP is owing to the poor statistics of the particle history. Below 1 MeV fluxes calculated by ANISN are lower than the flux by MCNP. This is partly due to neglecting the resonance self-shielding effect in the ANISN calculations in addition to the difference of nuclear data file in the case of GICX40.

(4) Effect of thermal neutron

Thermal neutron is not important in the shield design from the viewpoints of material irradiation damage. It plays, however, an important role to produce secondary gamma ray and therefore, it may affect on nuclear heat deposition.

Table 2.5 shows the thermal neutron flux and the secondary gamma ray flux in the shield calculated by MCNP. Case 1 is the normal MCNP run without special treatment of thermal neutron. Case 2 is the run of the more accurate treatment of thermal neutron (i.e. free-gas thermal treatment was applied). In Case 3, the energy cutoff was done at the neutron energy of 0.215 eV in order to examine the contribution of the thermal neutron. The maximum discrepancy of the thermal neutron flux between Case 1 and Case 2 is about 50 %. The thermal fluxes by the thermal treatment run are larger than those by the normal run except at the end of the shield (60 - 70 cm). In the rear part of the shield, however, the difference is not significant because of the large statistical errors. The gamma ray fluxes of the two cases do not differ much. From the results of Case 3, we can learn that the fraction of the gamma ray flux produced by the thermal neutron (here, $E < 0.215$ eV) varies from 10 % at the first wall to 40 % at the end of the shield.

Table 2.6 shows the gamma ray heat deposition in the shield. The results by the normal run and the thermal treatment run is almost the same (Case 1 and Case 2). The fractions of the gamma ray heat deposition

originated from the thermal neutron are about 25 % over the whole shield and over 50 % at the end of the shield (60 - 70 cm). From these results it is concluded that large error in the secondary gamma ray flux and heat deposition can be generated if the treatment of thermal neutron is not correct in the multi-group S_N calcutation.

2.2.2 Tungsten/water shield

(1) Neutron and gamma ray flux

Neutron fluxes and gamma ray fluxes are compared in Fig. 2.9 to Fig. 2.12 between the multi-group S_N calculations and the continuous energy Monte Carlo calculations in terms of ANISN to MCNP ratio. ANISN calculations using GICX40V4 and GICX50 were performed instead of GICXFNS and FSXJ3T1 because these liblaries do not include tungsten data. Neutron fluxes calculated by ANISN are smaller than those by MCNP, which is the similar tendency as the SS316/water case. In the tungsten/water case, however, discrepancies in 14 MeV neutron fluxes are larger than those in total neutron fluxes. The worst S_N/MC ratios in the total neutron fluxes are around 0.8 for GICX40, GICX40V4 and GICX50, and around 0.6 for VITAMIN-C, while those in the 14 MeV neutron fluxes are around 0.8 for GICX40 and 0.6 for GICX40V4, GICX50 and VITAMIN-C.

The gamma ray fluxes calculated using GICX40 are much smaller than those of MCNP. The worst S_N/MC ratio is around 0.4. While, the gamma ray fluxes calculated using GICX40V4 and GICX50 are much larger than that of MCNP. The worst ratios are around 3 and 4, respectively. Large difference is observed over all the thickness, even in the first wall region. Those calculated with VITAMIN-C are somewhat improved and the ratio is around 0.5.

The S_N/MC ratios in neutron and gamma ray fluxes at the position 40 cm from the first wall are summarized in Table 2.7. Accuracy of neutron fluxes does not seem to be improved by using the libraries based on the ENDF/B-IV instead of the ENDF/B-III file. The secondary gamma ray fluxes show large disagreement between these results.

(2) Nuclear heat deposition

The ANISN to MCNP ratios of the volume averaged nuclear heating rate by neutron and gamma ray are shown in Fig. 2.13 and Fig. 2.14, respectively. In this calculation, an additional zone of SS316 was placed behind W/water shield in order to evaluate heat deposition in SS316. The ANISN calculation using GICX40 underestimates gamma ray heating. Discrepancies in neutron heating are relatively small and the S_N/MC ratio is around 1.0.

Discrepancies in gamma ray heating is rather large and the worst ratio is around 0.5. While, the calculation using GICX40V4 overestimates gamma ray heating by a factor of 3. This tendency is the same as that of neutron and gamma ray fluxes mentioned above. Total heat deposition in the shield calculated by various methods and data are summarized in Table 2.8.
From these results, the following observations can be drawn;

1) Results of the neutron heating do not differ much between the different methods and data.
2) Results of the gamma ray heating show large disagreement between the results. Results of GICX40 is smaller than those of MCNP by a facto of 2.
3) Total heating calculated using the libraries generated by the NJOY code based on the ENDF/B-IV file is $\gtrsim$ 50 MeV per one DT neutron and this is clearly too high.

2.3 Conclusions

Main conclusions obtained from the analyses were summarized as follows;

(1) As for the SS316/H_2O shield, accuracy of neutron flux calculations was improved by using ENDF/B-IV and JENDL-3T instead of ENDF/B-III.
(2) The accuracy will be improved further if resonance self-shielded cross section data set is used.
(3) Gamma ray fluxes calculated with VITAMIN-C shows relatively good agreement with those of MCNP. They are, however, still underestimated and are consistent with the neutron flux calculations.
(4) As for the W/H_2O shield, no significant improvement was observed between ENDF/B-III and ENDF/B-IV in both neutron and gamma ray flux calculations.
(5) GICX40V4, GICX50 and GICXFNS accompany large errors (overestimation) in the gamma ray calculation and nuclear heat deposition. So attention should be paid when these are used in shielding design.
(6) GICX40 and VITAMIN-C can be applied to the shielding design. No kerma factors are, however, provided in VITAMIN-C at present. Correction against the underestimation of neutron and gamma ray flux must be done when using these libraries. Table 2.9 summarizes the correction factors.
(7) Secondary gamma ray cross section data and kerma factors are not included in FSXJ3T1(JENDL-3T) and therfore it can not be applied to the shielding design at present.

(8) If thermal neutron is not properly treated, large error can be generated in the secondary gamma ray flux and the heat deposition.

Table 2.1 Main Features of Cross Section Set Used in the Benchmark Calculations

Feature \ Cross Section set	GICX40[8]	GICX40V4[8]	GICX50[10]	GICXFNS[11]	FSXJ3T1[12]	VITAMIN-C[14]
Data File	ENDF/B-Ⅲ[9] POPO4 (gamma production)	ENDF/B-IV[9]	ENDF/B-IV	ENDF/B-IV	JENDL-3T[13]	ENDF/B-IV
Number of Neutron Groups (above 1 MeV)	42 (17)	42 (17)	42 (17)	135 (60)	125 (64)	171 (59)
Number of Gamma ray Groups	21	21	21	21	—	36
Processing Code	RADHEAT	NJOY	NJOY	NJOY	PROF.GROUCH -G/B	AMPX
Weight Function	1/E	Spectrum in fusion blanket	1/E	Constant	1/E + Maxwell	Maxwell + Fission + 1/E + Fusion
Self-shielding	Infinite dilution	Infinite dilution	Infinite dilution	Infinite dilution	Infinite dilution	Infinite dilution
Kerma factors	yes	yes	yes	yes	none	none

Table 2.2 Number Densities of Materials used for Shielding Benchmark Calculations

Material	Element	Number Density (n/cm^3)
Plasma	^{2}H	1.0×10^{13}
316SS	Mo	1.255×10^{21}
	Cr	1.575×10^{22}
	Ni	9.848×10^{21}
	Fe	5.909×10^{22}
H_2O	H	6.686×10^{22}
	O	3.343×10^{22}
W	^{182}W	1.720×10^{22}
	^{183}W	9.254×10^{21}
	^{184}W	1.976×10^{22}
	^{186}W	1.821×10^{22}

Table 2.3 Comparison of the Neutron and Gamma Ray Fluxes Calculated with the Different Cross Section Libraries (normalized to the results of MCNP) at the Position 60 cm from the First Wall ($SS316/H_2O$ shield)

Methods	MCNP (ENDF/B-IV)	ANISN					
		GICX40	GICX40V4	GICX50	GICXFNS	FSXJ3T1	VITAMIN-C
14 MeV Neutron	1	1.31	0.814	1.04	1.03	0.938	0.831
Fast Neutron (E > 0.1 MeV)	1	0.562	0.586	0.721	0.760	0.714	0.766
Total Neutron	1	0.540	0.482	0.645	0.708	0.716	0.729
Thermal Neutron	1	0.469	0.379	0.285	0.759	0.772	1.12
Gamma Ray	1	0.258	1.04	1.57	2.30	—	0.763
Neutron Heat Deposition (60~70 cm)	1	0.732	0.625	0.867	0.627	—	—
Gamma Heat Deposition (60~70 cm)	1	0.299	0.728	1.01	1.44	—	—

14 MeV Neutron Energy
15(14.1)-13.72 MeV for (MCNP), GICX40, GICX40V4, GICX50
14.218 -13.967 MeV for GICXFNS
14.1 -13.88 MeV for FSXJ3T1
14.19 -13.84 MeV for VITAMIN-C

Thermal Energy
<0.215 eV for MCNP, GICX40, GICX40V4, GICX50, GICXFNS
<0.3244 eV for FSXJ3T1
<0.414 eV for VITAMIN-C

Table 2.4 Nuclear Heat Deposition in $SS316/H_2O$ Shield Calculated by Various Method (MeV/DT Neutron)

Methods	MCNP (ENDF/B-IV)	ANISN				IEBM*
		GICX40	GICX40V4	GICX50	GICXFNS	
Neutron Heating	4.12	4.21	5.41	4.14	3.80	—
Gamma Heating	16.4	10.4	23.6	39.6	25.1	—
n + g	20.5	14.6	29.0	43.7	28.9	19.7

* Integral Energy Balance Method
(Using the neutron flux calculated by GICX40V4)

$$H_t = E_{in} + \Sigma \Sigma R_{ij} Q_{ij} \qquad (2)$$

(see the text)

Table 2.5 Comparison of Thermal Neutron Flux and Gamma Ray Flux with/without Thermal Treatment in MCNP and Contribution of Thermal Neutron to Secondary Gamma Ray Production

(1) Thermal Neutron Flux

Distance from First Wall (cm)	Case 1 (Without thermal treatment)	Case 2 (With thermal treatment)
0	2.02-4* (0.019)**	2.42-4 (0.023)
10	1.48-4 (0.014)	1.81-4 (0.019)
20	7.08-5 (0.020)	8.58-5 (0.025)
30	2.65-5 (0.035)	3.23-5 (0.039)
40	8.28-6 (0.058)	9.50-6 (0.063)
50	2.20-6 (0.097)	2.60-6 (0.111)
60	6.71-7 (0.207)	6.20-7 (0.184)
70	4.21-8 (0.389)	2.82-8 (0.413)

(2) Gamma Ray Flux

Distance from First Wall (cm)	Case 1 (Without thermal treatment)	Case 2 (With thermal treatment)	Case 3 (Energy Cutoff at 0.215eV)
0	6.34-3 (0.007)	6.33-3 (0.008)	5.47-3 (0.008), 11%***
10	2.73-3 (0.007)	2.77-3 (0.008)	2.21-3 (0.009), 20%
20	9.75-4 (0.011)	9.89-4 (0.013)	7.30-4 (0.015), 26%
30	3.11-4 (0.019)	3.18-4 (0.021)	2.13-4 (0.026), 33%
40	9.91-5 (0.032)	1.02-4 (0.039)	6.71-5 (0.050), 34%
50	2.70-5 (0.054)	2.61-5 (0.066)	1.77-5 (0.089), 32%
60	7.70-6 (0.106)	8.00-6 (0.134)	4.81-6 (0.149), 40%
70	6.08-7 (0.179)	9.00-7 (0.244)	5.65-7 (0.238), 37%

* Read as 2.02×10^{-4}
** (fractional standard deviation)
*** Contribution ratio of thermal neutron

Table 2.6 Comparison of Gamma Ray Heat Deposition with/without Thermal Treatment in MCNP and Contribution Ratio of Thermal Neutron to Gamma Ray Heat Deposition

	Case 1 (Without thermal treatment)	Case 2 (With thermal treatment)	Case 3 Energy cutoff at 0.215 eV
0 - 10	9.55* (0.004)	9.60 (0.004)	7.66 (0.004), 20%**
10 - 20	4.27 (0.006)	4.33 (0.006)	3.01 (0.007), 30%
20 - 30	1.68 (0.010)	1.70 (0.010)	1.07 (0.012), 37%
30 - 40	0.585 (0.017)	0.593 (0.017)	0.354 (0.021), 40%
40 - 50	0.197 (0.031)	0.191 (0.031)	0.113 (0.037), 41%
50 - 60	0.0639 (0.055)	0.0563 (0.057)	0.0344 (0.067), 39%
60 - 70	0.0147 (0.106)	0.0173 (0.108)	0.00848 (0.136), 51%
0 - 70	16.36 MeV	16.49 MeV	12.25 MeV , 26%

* Heat deposition per one DT neutron
** Contribution ratio of thermal neutron

Table 2.7 Comparison of the Neutron and Gamma Ray Flux Calculated with the Different Cross Section Libraries (normalized to the results of MCNP) at the Position 40 cm from the First Wall (W/H_2O Shield)

Methods	MCNP (ENDF/B-IV)	ANISN			
		GICX 40	GICX40V4	GICX50	VITAMIN-C
14 MeV Neutron	1	0.859	0.687	0.693	0.598
Fast Neutron (E>0.1MeV)	1	0.960	0.986	0.955	0.648
Total Neutron	1	0.871	0.976	0.892	0.604
Gamma Ray	1	0.409	1.22	0.783	0.535
Neutron Heat Deposition (40-50cm)	1	0.974	0.826	0.966	———
Gamma Heat Deposition (40-50cm)	1	0.471	1.18	0.839	———

Table 2.8 Nuclear Heat Deposition in W/H_2O shield Calculated by the Various Methods (MeV/DT Neutron)

Methods	MCNP (ENDF/B-IV)	ANISN		
		GICX40	GICX40V4	GICX50
Neutron Heating	1.50	1.57	0.969	1.52
Gamma Heating	18.8	10.3	48.4	63.6
n + g	20.3	11.9	49.4	65.1

Table 2.9 Correction Factors for Calculation Error due to Multi-Group S_N Methods Applied to the Inboard Shielding Properties (Shield Thickness ~60 cm)

	$SS316/H_2O$		W/H_2O	
	GICX40	VITAMIN-C	GICX40	VITAMIN-C
Neutron flux	2	1.4	1.3	2
Gamma ray flux	4	1.4	3	2
Neutron heating	1.4	——	~ 1	——
Gamma ray heating	4	——	2.4	——
Total heat deposition in shield	1.4	——	1.7	——

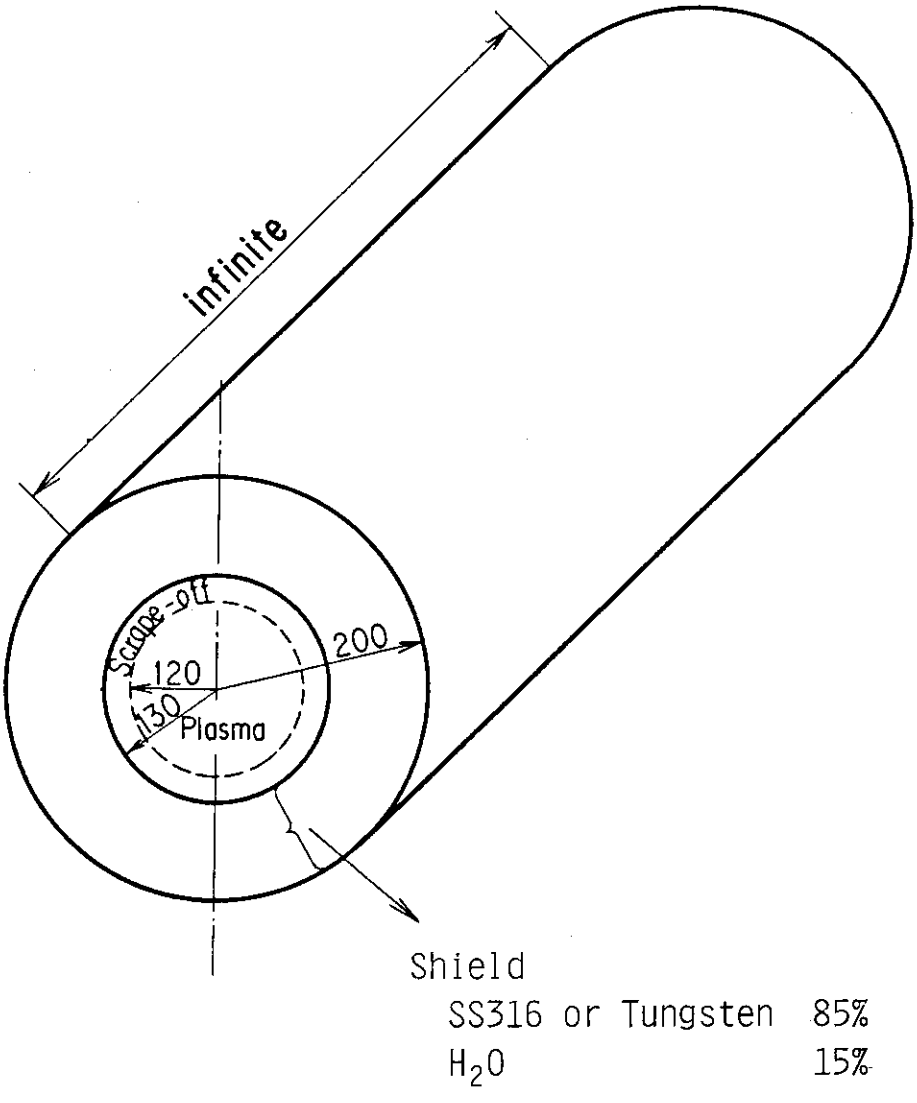

Fig. 2.1 Infinite Cylindrical Model for the First Benchmark Calculation

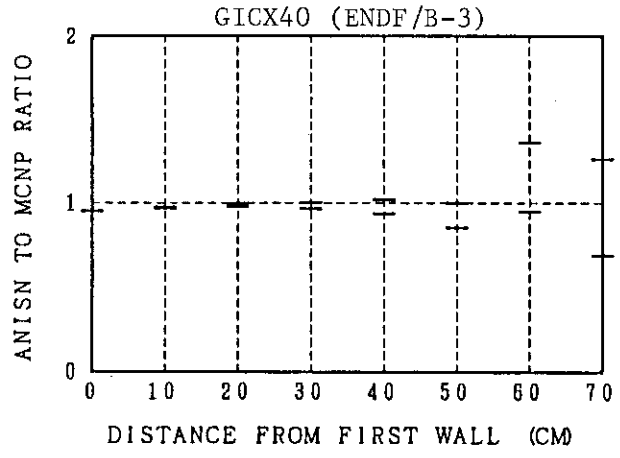

(a) 14 MeV Neutron

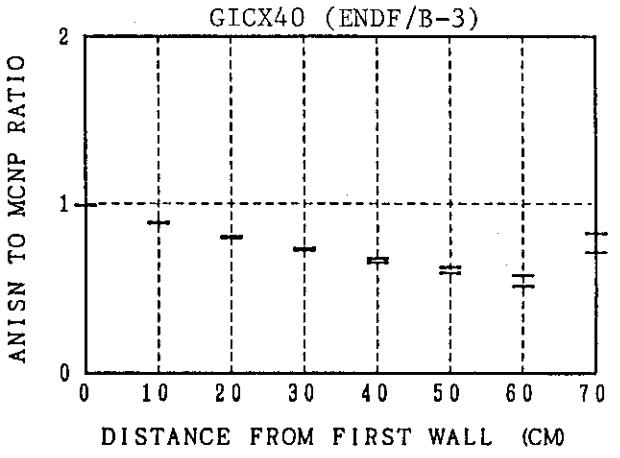

(b) Fast Neutron

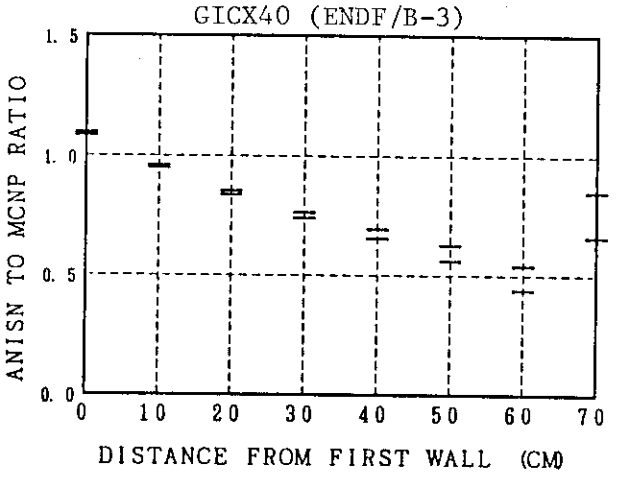

(c) Total Neutron

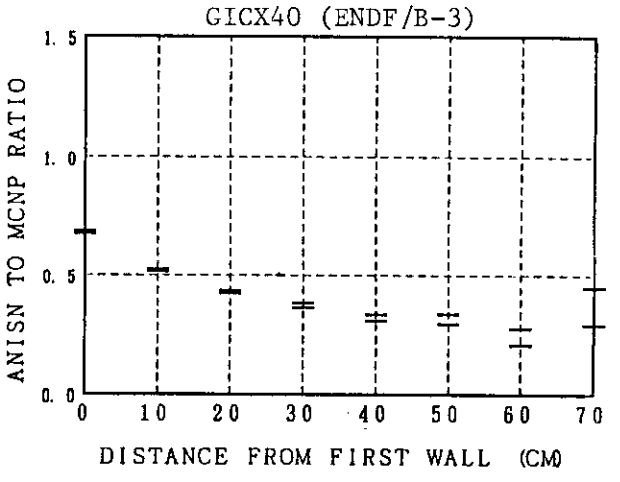

(d) Gamma Ray

Fig. 2.2 Comparison of Neutron and Gamma Ray Fluxes in SS316/H_2O Shield between ANISN/GICX40 and MCNP
Two bars at each position represent the confidence interval of the one standard deviation (1σ).

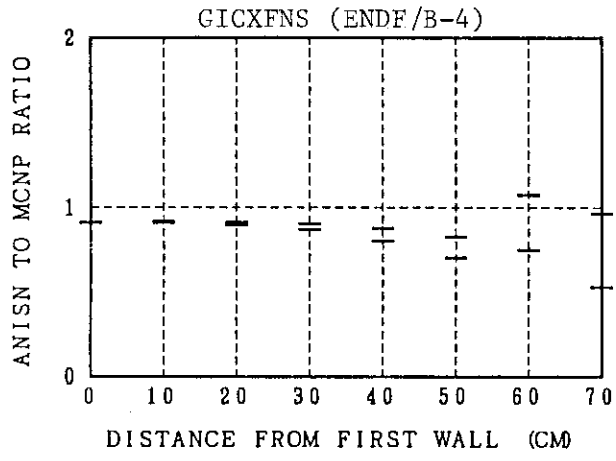

(a) 14 MeV Neutron

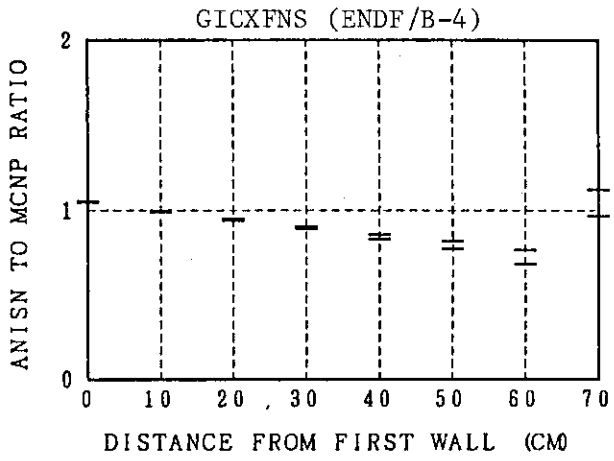

(b) Fast Neutron

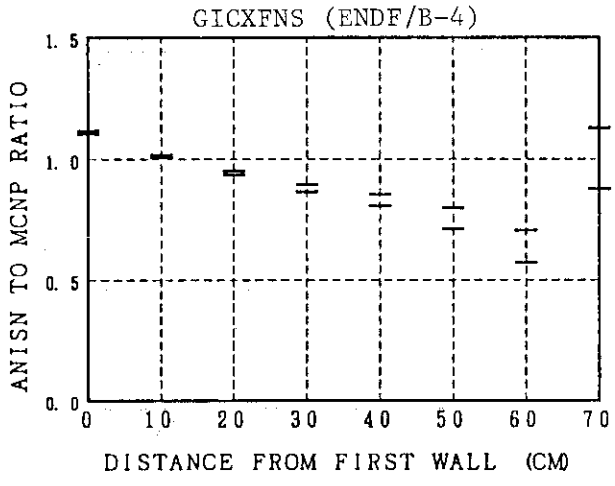

(c) Total Neutron

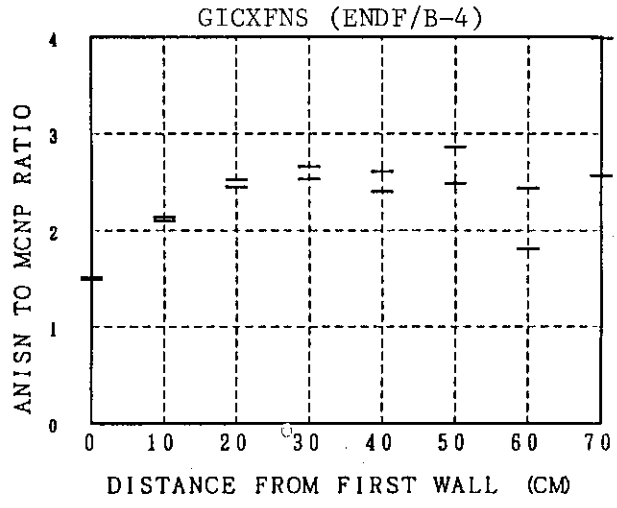

(d) Gamma Ray

Fig. 2.3 Comparison of Neutron and Gamma Ray Fluxes in SS316/H_2O Shield between ANISN/GICXFNS and MCNP

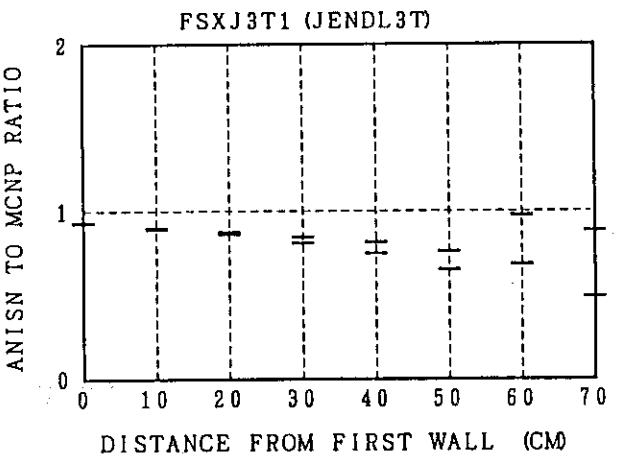

(a) 14 MeV Neutron

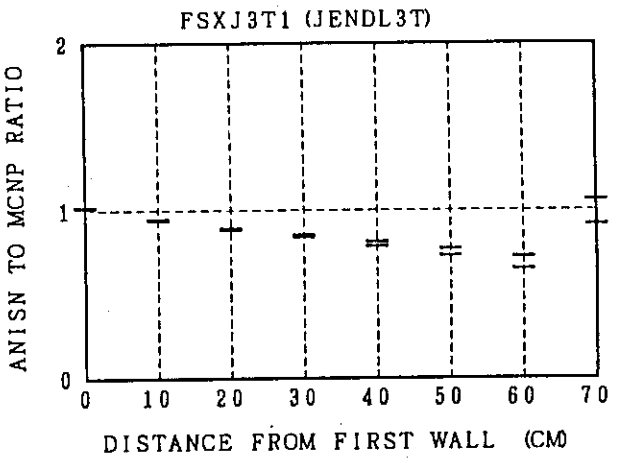

(b) Fast Neutron

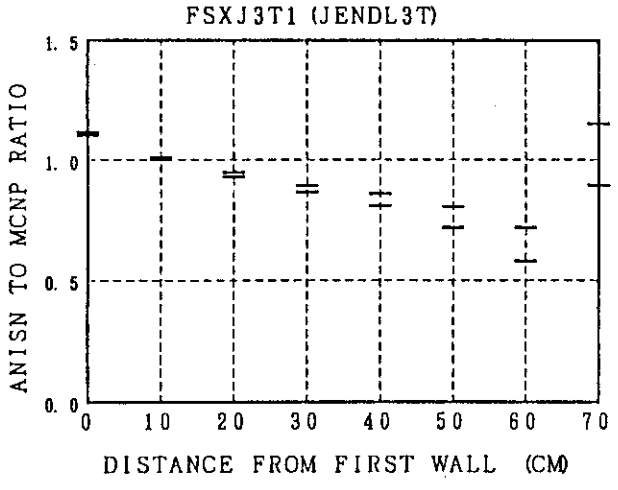

(c) Total Neutron

Fig. 2.4 Comparison of Neutron and Gamma Ray Fluxes in SS316/H_2O Shield between ANISN/FSXJ3T1 and MCNP

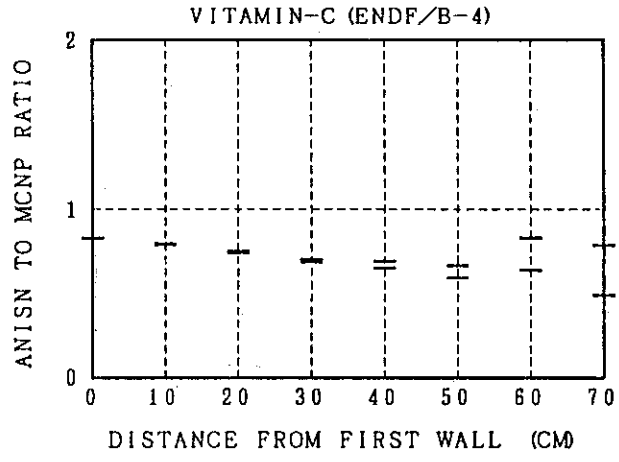

(a) 14 MeV Neutron

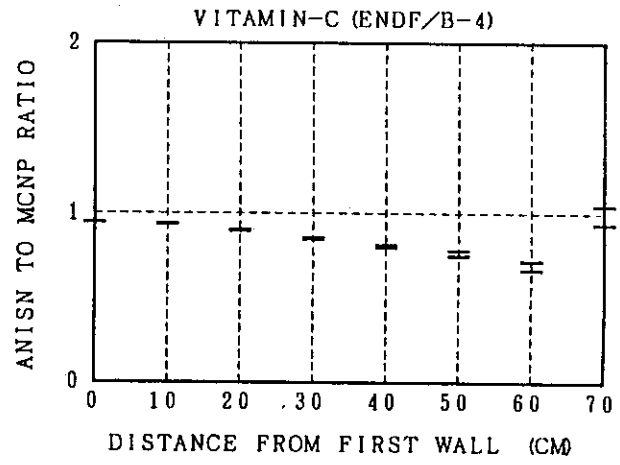

(b) Fast Neutron

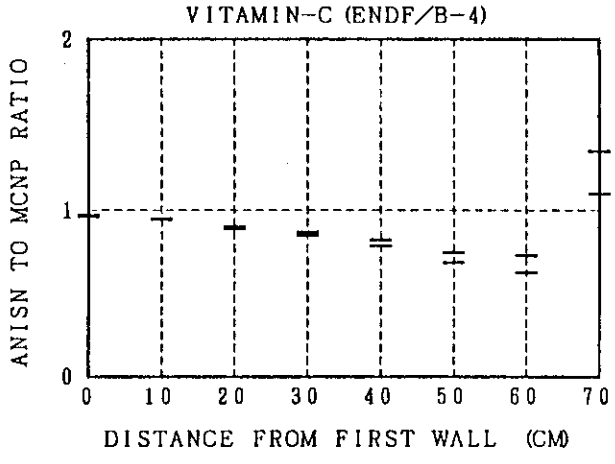

(c) Total Neutron

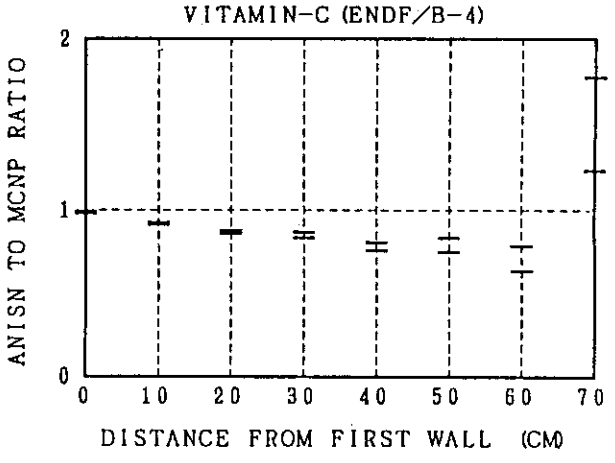

(d) Gamma Ray

Fig. 2.5 Comparison of Neutron and Gamma Ray Fluxes in SS316/H_2O Shield between ANISN/VITAMIN-C and MCNP

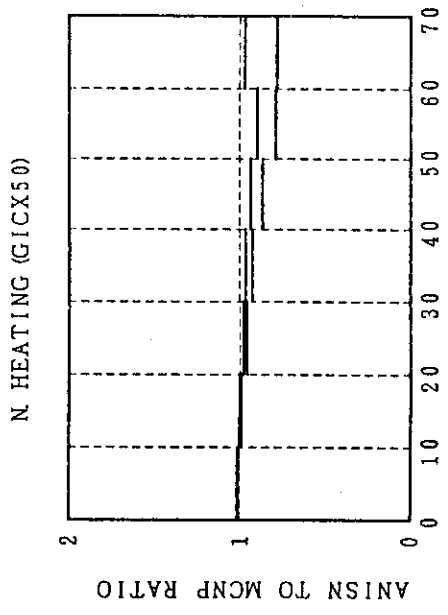

(a) Neutron Heating

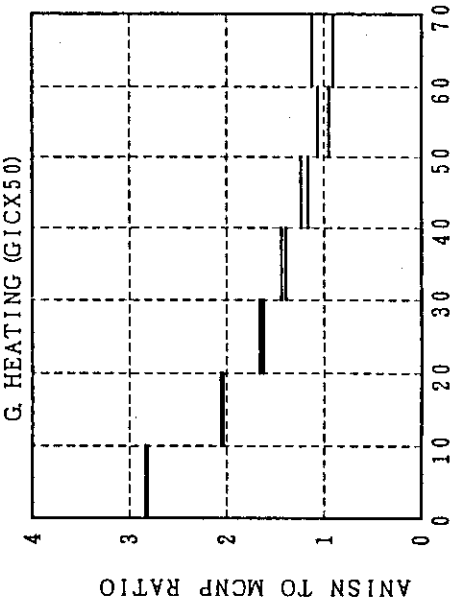

(b) Gamma Ray Heating

Fig. 2.7 Comparison of Neutron and Gamma Ray Heating in SS316/H_2O Shield between ANISN/GICX50 and MCNP

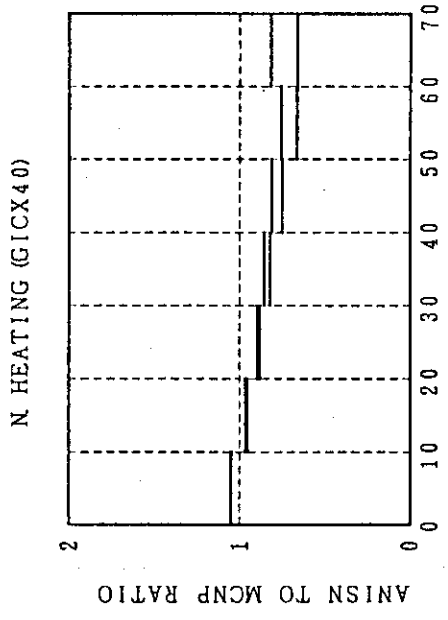

(a) Neutron Heating

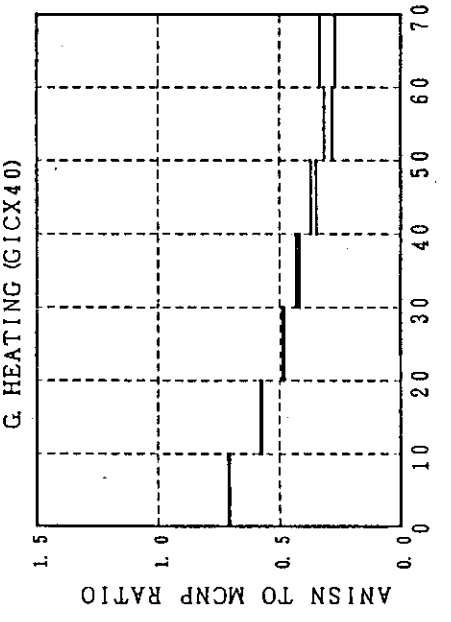

(b) Gamma Ray Heating

Fig. 2.6 Comparison of Neutron and Gamma Ray Heating in SS316/H_2O Shield between ANISN/GICX40 and MCNP

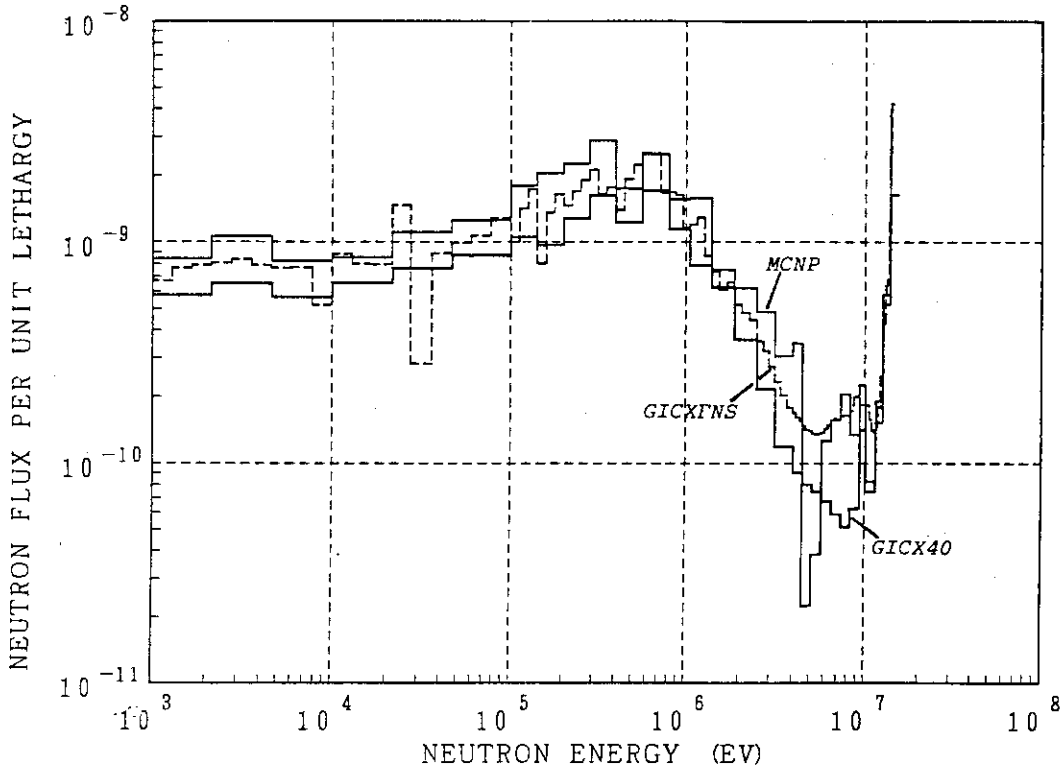

Fig. 2.8 Neutron Energy Spectra at the Position 50 cm from the First Wall (SS316/H_2O Shield)

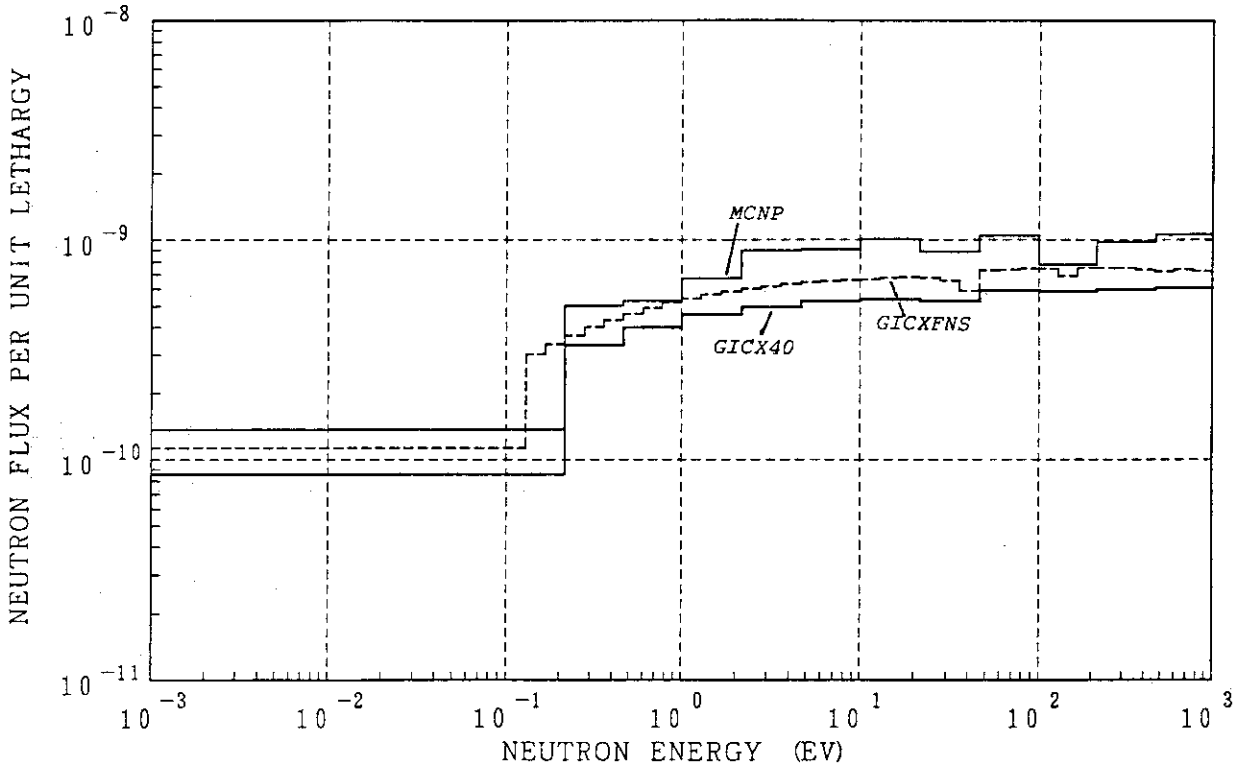

Fig. 2.8 (Cont'd)

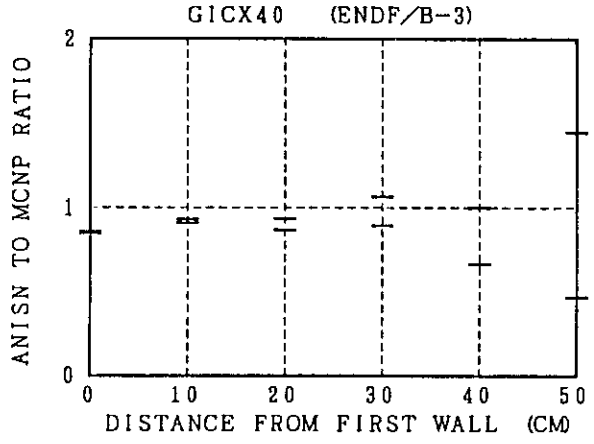

(a) 14 MeV Neutron

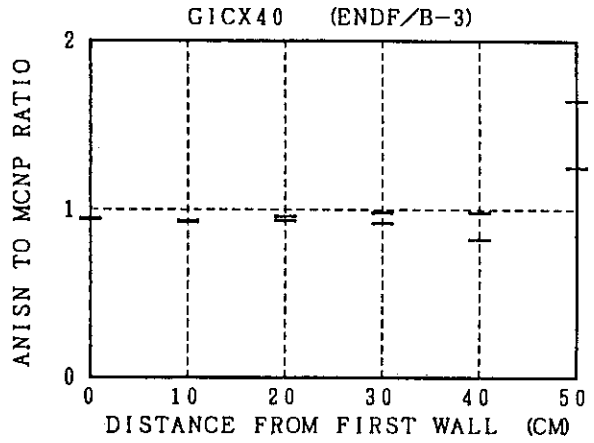

(b) Fast Neutron

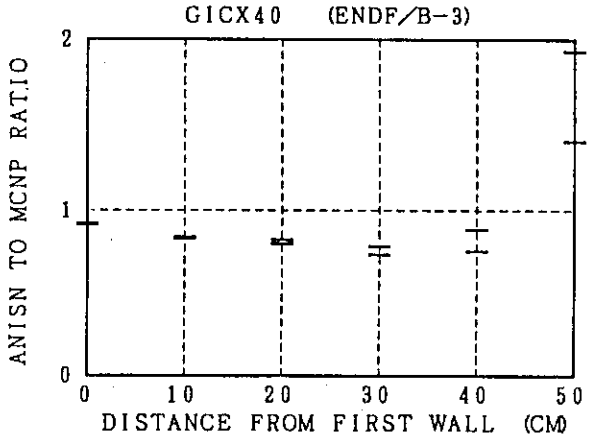

(c) Total Neutron

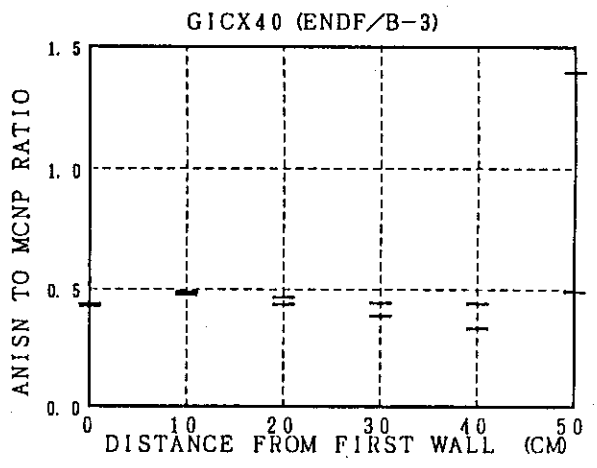

(d) Gamma Ray

Fig. 2.9 Comparison of Neutron and Gamma Ray Fluxes in W/H_2O Shield between ANISN/GICX40 and MCNP
Two bars at each position represent the confidence interval of the one standard deviation (1σ).

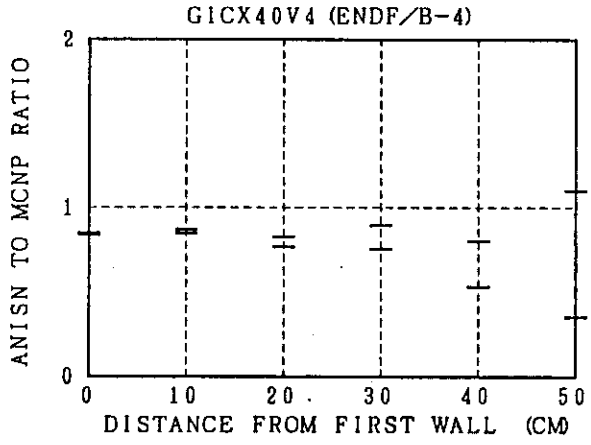

(a) 14 MeV Neutron

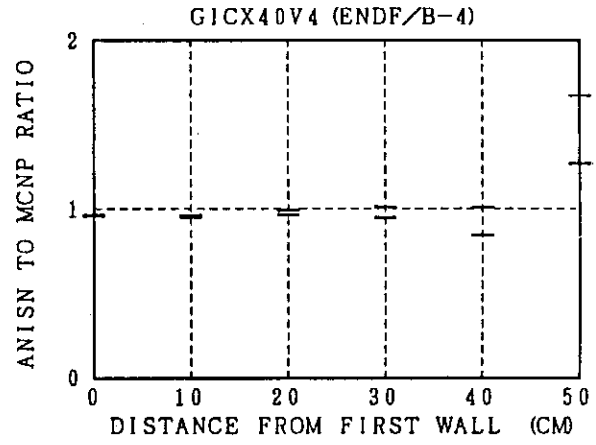

(b) Fast Neutron

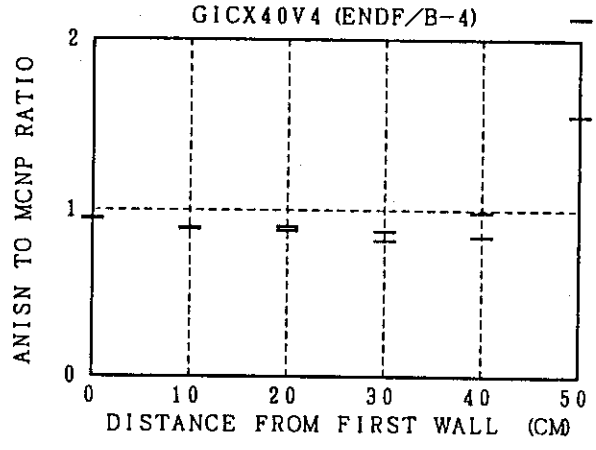

(c) Total Neutron

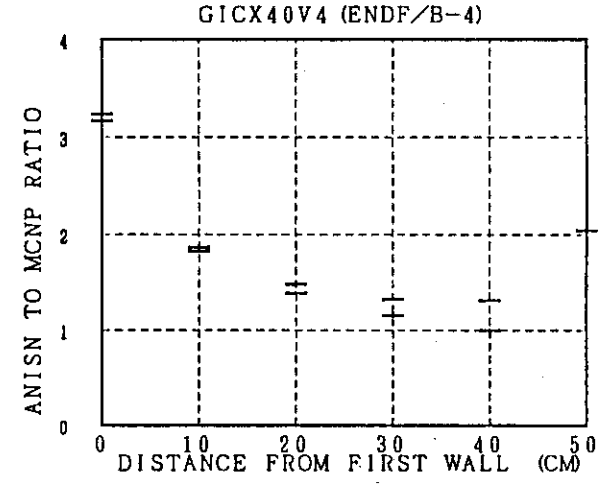

(d) Gamma Ray

Fig. 2.10 Comparison of Neutron and Gamma Ray Fluxes in W/H_2O Shield between ANISN/GICX40V4 and MCNP

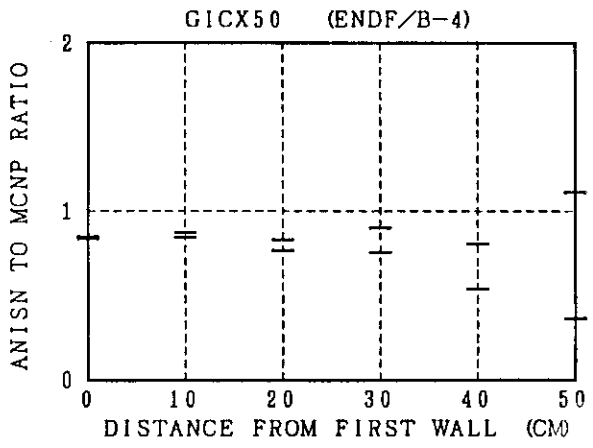

(a) 14 MeV Neutron

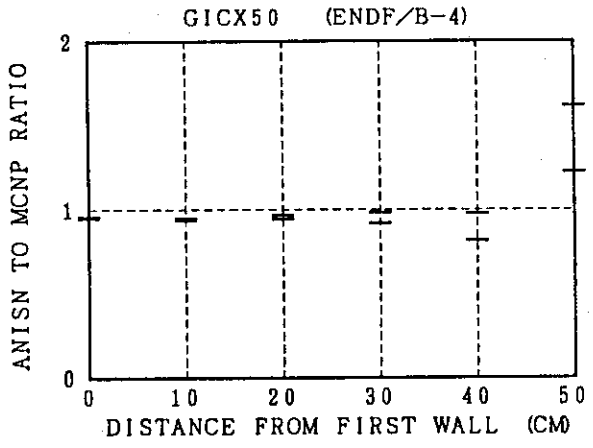

(b) Fast Neutron

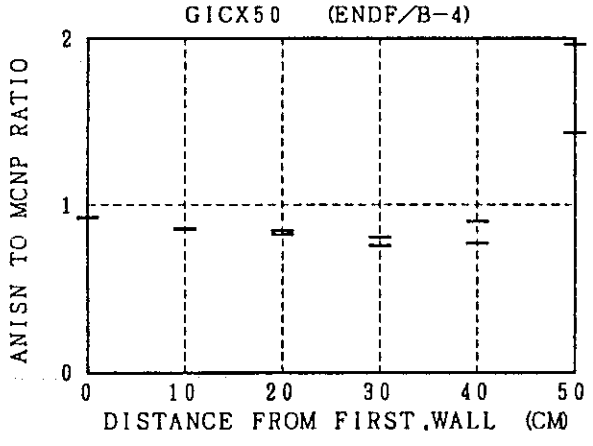

(c) Total Neutron

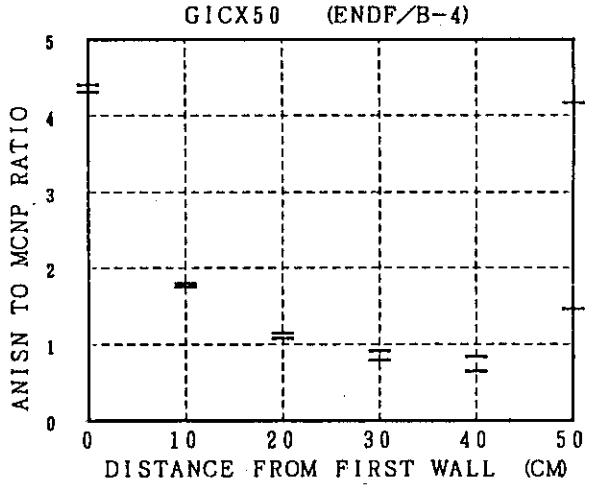

(d) Gamma Ray

Fig. 2.11 Comparison of Neutron and Gamma Ray Fluxes in W/H_2O Shield between ANISN/GICX50 and MCNP

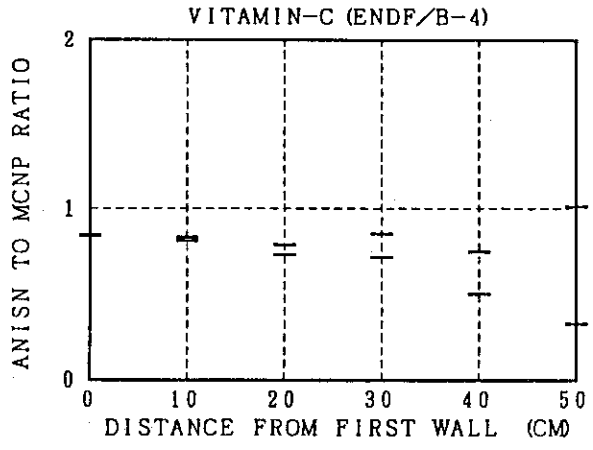

(a) 14 MeV Neutron

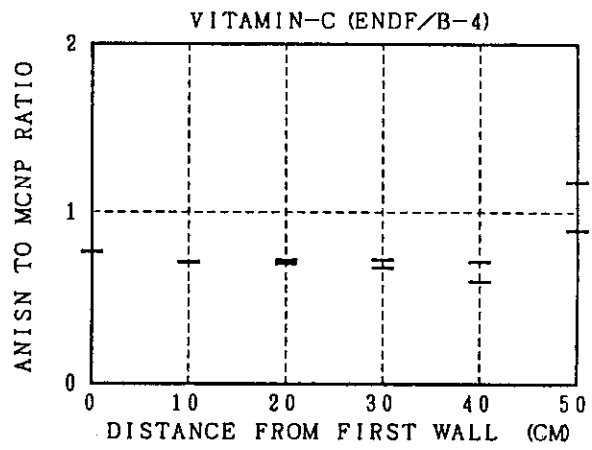

(b) Fast Neutron

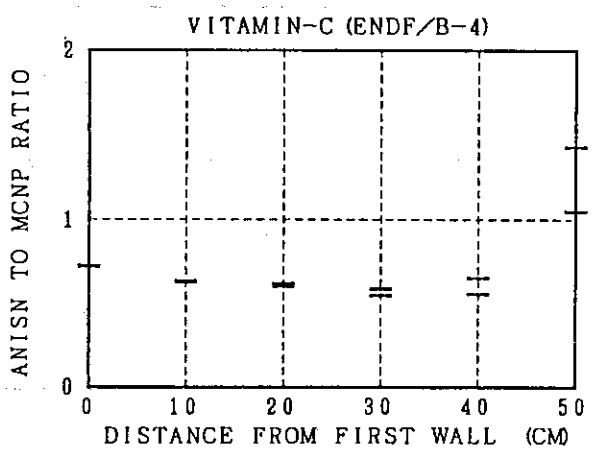

(c) Total Neutron

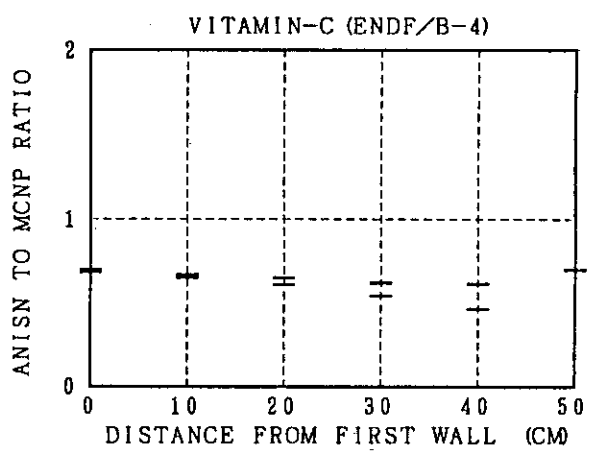

(d) Gamma Ray

Fig. 2.12 Comparison of Neutron and Gamma Ray Fluxes in W/H_2O Shield between ANISN/VITAMIN-C and MCNP

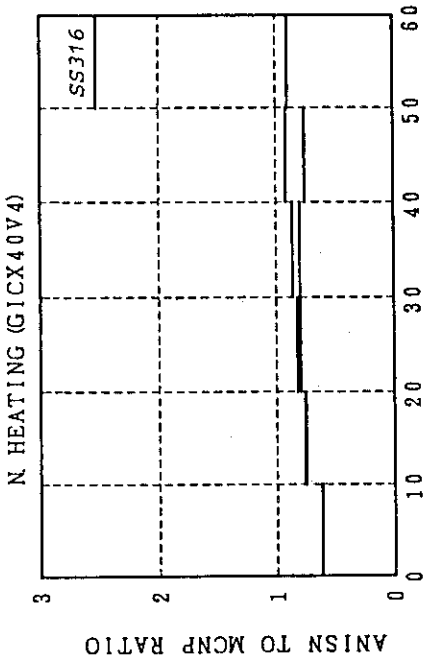

(a) Neutron Heating

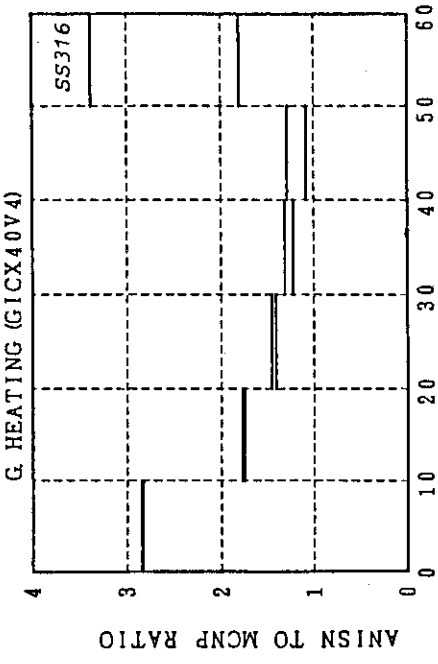

(b) Gamma Ray Heating

Fig. 2.14 Comparison of Neutron and Gamma Heating in W/H_2O Shield between ANISN/GICX40V4 and MCNP

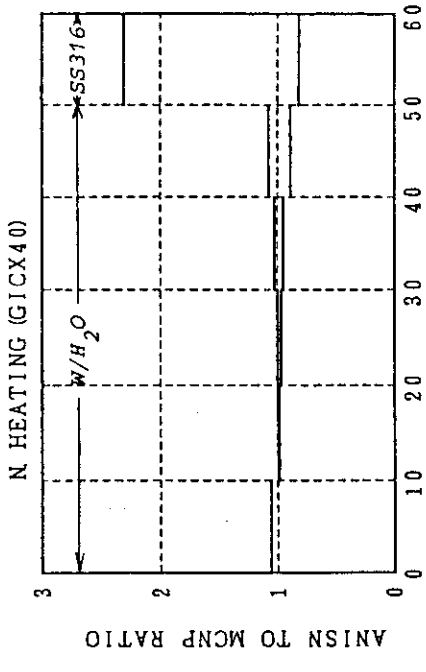

(a) Neutron Heating

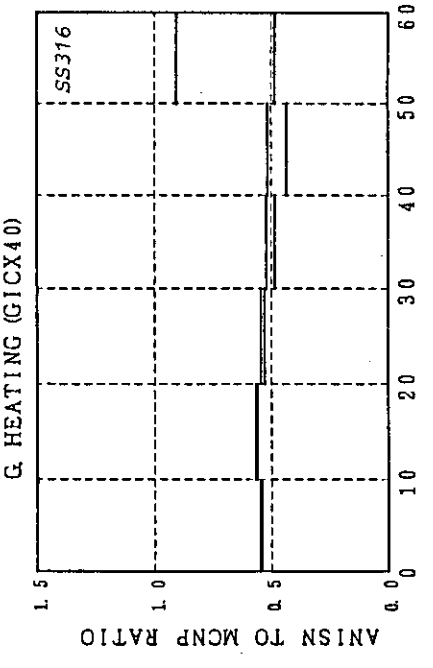

(b) Gamma Ray Heating

Fig. 2.13 Comparison of Neutron and Gamma Ray Heating in W/H_2O Shield between ANISN/GICX40 and MCNP

3. Accuracy Evaluation of Iron Cross Section Data

3.1 Method of Evaluation

Transmission experiment using 14 MeV neutron source through iron sphere was analyzed using the current cross section data and the results were compared with the measured values, because iron is the most basic element in the shield. The experiment analyzed is that performed by Hertel et.al.[17]. Geometry, dimensions and material compositions are shown in Table 3.1 and Table 3.2.

Analytical calculations were performed by ANISN using GICX40, GICXFNS, FSXJ3T1 and VITAMIN-C, and by MCNP using ENDF/B-IV and JENDL-3T. All calculations were performed using the one-dimensional sphere model with the isotropic and monoenergetic neutron source region in its center as shown in Fig. 3.1. The ANISN calculation used the P_5 (P_3 for VITAMIN-C) - S_{16} approximation. Surface crossing estimator was used in the MCNP calculations to evaluate leakage neutron from the sphere. Measured and calculated results were compared in terms of the number of leakage neutron and leakage neutron energy spectra.

The measured value per one source neutron is related to the calculated value by the following equation[18];

$$\phi_s = \frac{4\pi d^2 \int_0^{\pi} \phi(d,E,\theta)\ \cos\theta \cdot 2\pi\ \sin\theta d\theta}{\int_0^{\infty} Q(E)\ dE} \tag{3}$$

$$= 4\pi d^2\ \phi_t\ (d,E) \Big/ \int_0^{\infty} Q(E)\ dE \tag{4}$$

where,

d : Radius of sphere (cm)

$\phi(d,E,\theta)$: Angular flux on the sphere surface ($n/cm^2/MeV/Sr$)

$\int_0^{\infty} Q(E)\ dE$: Number of neutrons emitted from the source target

$\phi_t(d,E)$: Net neutron current on the sphere surface ($n/cm^2/MeV$)

3.2 Calculation Results

The measured and calculated leakage neutron spectra are compared in Fig. 3.2. The calculated results were not smoothed by the detector efficiency. The results by ANISN/GICX40 is much smaller than the other

calculated results and the measurement in the energy range of 3 - 10 MeV. Other three calculted results (ANISN/GICXFNS, FSXJ3T1 and MCNP) agree well, but they are still smaller than the measurements in almost all the energy range, especially below 5 MeV.

The number of neutron leakage from the sphere as calculated and measured is tabulated in Table 3.3. They show good agreement above 10 MeV. In the range of 5 - 10 MeV, the calculations underpredict the measurements, although the disagreement is not larger than the experimental error except the results by GICX40. The calculated results are much smaller than the measurements below 5 MeV. Consequently calculated total neutron leakage above 1 MeV underpredict the measurement by a factor of >2 for MCNP and by a factor of 3 to 4 for ANISN.

3.3 Conclusions

Main conclusions obtained from the analysis were summarized as follows;

(1) The E/C ratio was improved by the MCNP calculation compared to the ANISN calculations. The calculations grossly underestimate the measurements. The E/C ratio is smaller than 0.5 for the fast neutron with the energy greater than 1 MeV.

(2) ENDF/B-IV and JENDL-3T give almost the same results. ENDF/B-III gives the larger discrepancy.

(3) Since the experimental error is also rather large, other similar experiments should be analyzed to conclude the accuracy of the current data.

(4) Since this experiment is not for the purpose of shielding benchmark, it is necessary to perform shielding benchmark experiment. It should include thicker test material (70 ~ 100 cm), actual shielding material/configuration (SS316, tungsten, water) and measurment of low energy neutron and secondary gamma ray.

Table 3.1 Physical Properies of the Iron Spherical Shell of Hertel's Experiment[17]

Outer radius (cm)	38.10
Inner radius (cm)	7.65
Density (g/cm^3)	7.87
Number density (nuclei/b·cm)	0.0849
Shell thickness (mfp)	
2-MeV neutrons	6.9
14-MeV neutrons	6.5

Table 3.2 Atomic Number Densities for Iron of Hertel's Experiment

Element	Weight fraction (%)	Atomic compositions (atoms/cm^3)
Fe	99.3046	8.4280×10^{22}
C	0.21	8.21×10^{20}
Mn	0.47	4.05×10^{20}
P	0.013	1.99×10^{19}
S	0.0024	3.5×10^{18}
Density	7.87 g/cm^3	—

Table 3.3 Measured and ANISN & MCNP Calculated Neutron Leakage for the iron Spherical Shell Containing the D-T Source

Energy Region	Measurements (n/source n)	MCNP Calculation (n/source n)	ANISN Calculations (n/source n)			
	Hertel's Work[17]	ENDF/B-IV 50,000 JENDL-3T 100,000	FSXJ3T1 $P_5 - S_{16}$	GICX40 $P_5 - S_{16}$	GICFNS $P_5 - S_{16}$	VITAMIN-C $P_3 - S_{16}$
> 10	$(2.0 \pm 0.1) \times 10^{-2}$	$(1.91 \pm 0.06) \times 10^{-2}$ $(1.70 \pm 0.04) \times 10^{-2}$	1.62×10^{-2}	1.97×10^{-2}	1.78×10^{-2}	1.81×10^{-2}
5 to 10	$(5.3 \pm 2.2) \times 10^{-3}$	$(3.87 \pm 0.24) \times 10^{-3}$ $(2.67 \pm 0.14) \times 10^{-3}$	2.66×10^{-3}	9.65×10^{-4}	3.36×10^{-3}	3.42×10^{-3}
2.23 to 5.0	$(2.3 \pm 0.1) \times 10^{-2}$	$(1.01 \pm 0.04) \times 10^{-2}$ $(1.14 \pm 0.03) \times 10^{-2}$	1.03×10^{-2}	4.19×10^{-3}	9.56×10^{-3}	9.96×10^{-3}
1.0 to 2.23	$(1.9 \pm 0.1) \times 10^{-1}$	$(6.62 \pm 0.10) \times 10^{-2}$ $(5.01 \pm 0.06) \times 10^{-2}$	3.54×10^{-2}	3.38×10^{-2}	4.02×10^{-2}	4.56×10^{-2}
		10.0 ~ 14.01 MeV 5.028 ~ 10.0 MeV 2.23 ~ 5.028 MeV 1.054 ~ 2.23 MeV (FSXJ3T1)	10.5 ~ 15 MeV 5.99 ~ 10.5 MeV 2.5 ~ 5.099 MeV 1.058 ~ 2.5 MeV (GICX40)	10.50 ~ 14.218 MeV 5.099 ~ 10.5 MeV 2.27 ~ 5.099 MeV 1.058 ~ 2.27 MeV (GICXFNS)	10.0 ~ 14.19 MeV 4.966 ~ 10.0 MeV 2.231 ~ 4.966 MeV 1.003 ~ 2.231 MeV (VITAMIN-C)	

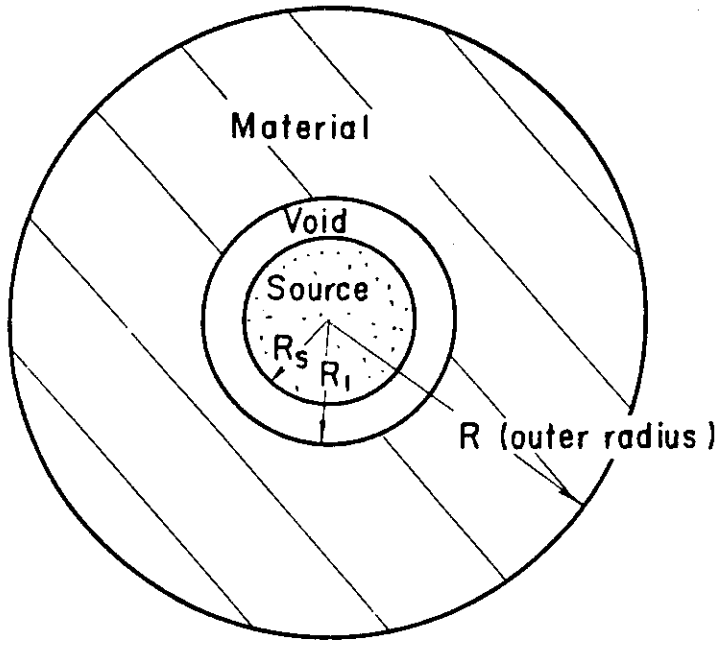

Material	Source(R_s)	R_1	R
Iron	1.03	7.65	38.1

Fig. 3.1 Calculational Model for One-Dimensional Geometry (unit: cm)

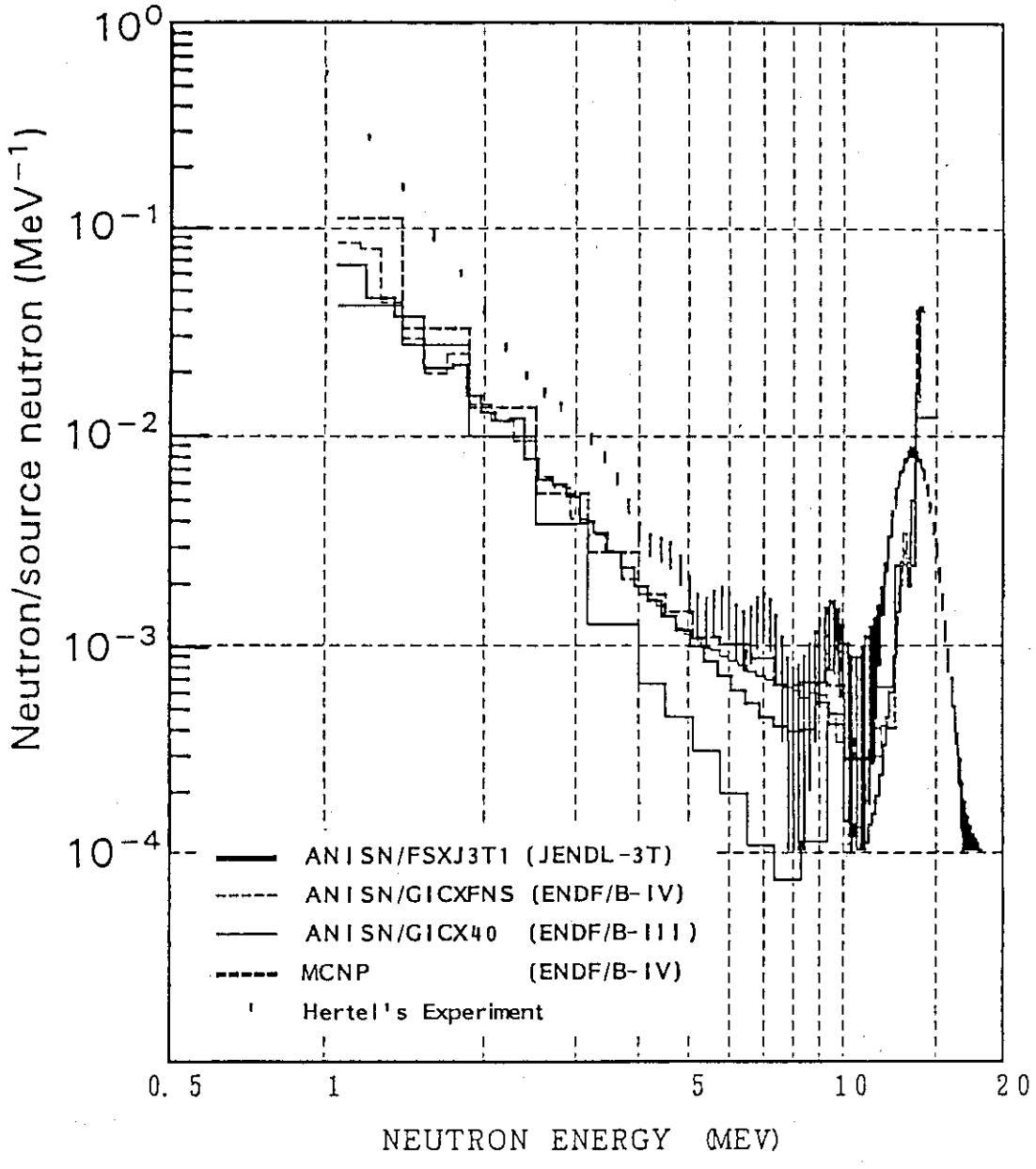

Fig. 3.2 Comparison of the Leakage Neutron Spectra from the Iron Sphere between the Measurement and the Calculations.

4. Uncertainty Due To Structural Heterogeneity

4.1 Calculation Method

Influence of the heterogeneous representation of the shield structure was invetigated by comparing with the homogeneous representation. The one-dimensional homogeneous model is shown in Fig. 2.1. The one-dimensional heterogeneous model of alternating layers of SS316 and water, which is closer to the actual mechanical design, is shown in Fig. 4.1. Calculation parameters for ANISN using GICX40 are the same as the homogeneous case as described in the section 2.1.

4.2 Calculation Results

Neutron and gamma ray fluxes at the end of the shield calculated by ANISN using the heterogeneous model and the homogeneous one are compared in Table 4.1. Attenuation of the 14 MeV neutron flux is not affected by the geometrical representation. The fast and total neutron fluxes by the heterogeneous model are larger than those by the homogeneous model by a factor of ~2. The thermal neutron flux by the heterogeneous model is much smaller than that by the homogeneous model, but it is strongly dependent on the geometry. The gamma ray flux by the heterogeneous model is smaller than by the homogeneous model by about 10 %, but it is also geometry dependent.

Heat deposition in the shield calculated by ANISN using the two models are compared in Table 4.2. The heat deposition in SS316 by the heterogeneous model is smaller than the homogeneous one by 10 %. While, heat deposition in water is larger by a factor of 2. The total heat depositions in the shield (SS316-85 %, water-15 %) do not differ much. The discrepancy is smaller than 2 %, though the neutron heating by the heterogeneous model is larger by 20 % and the gamma heating is smaller by 10 %.

The similar comparison of the MCNP results is summarized in Table 4.3. Although the statistics of the particle history is poor, the same tendency as the ANISN results is observed.

4.3 Conclusions

Main conclusions obtained from the analysis were summarized as follows;

(1) The homogeneous model underpredicts the fast neutron flux at the end of the shield by a factor of 2. Therefore, attention should be paid when using the homogeneous model in the shielding design.

(2) Destribution of thermal neutron and secondary gamma ray in shield is strongly dependent on the material configuration in particular in water region. Though it may not affect the shielding performance, it may affect neutronics performances, such as tritium production rate, which is not the subject of this report.

(3) Further investigation should be required for the other shield configuration and combination of materials to define the heterogeneous effect.

Table 4.1 Comparison of Neutron and Gamma Ray Fluxes between the Homogeneous Model and the Heterogeneous Model at the Position 69.5 cm from the First Wall ($SS316/H_2O$)

	Hetero./Homo. Ratio
14 MeV Neutron Flux	1.01
Fast Neutron Flux	2.07
Thermal Neutron Flux	0.0279
Total Neutron Flux	1.70
Gamma Ray Flux	0.894

The calculation was performed by ANISN/GICX40.

Table 4.2 Comparison of Neutron and Gamma Ray Heat Deposition per One DT Neutron in $SS316/H_2O$ Shield between the Homogeneous Model and the Heterogeneous Model

Material		Hetero. (MeV)	Homo. (MeV)	Hetero./Homo. Ratio
SS316	Neutron	2.43	2.75	0.884
	Gamma Ray	8.91	10.2	0.874
	Total	11.34	12.95	0.876
H_2O	Neutron	2.57	1.46	1.76
	Gamma Ray	0.430	0.212	2.03
	Total	3.0	1.672	1.79
$SS316/H_2O$ Mixture	Neutron	5.0	4.21	1.19
	Gamma Ray	9.34	10.4	0.898
	Total	14.34	14.6	0.982

The calculation was performed by ANISN/GICX40.

Table 4.3 Comparison of Neutron and Gamma Ray Fluxes at the Outer Surface of SS316/H_2O Shield and Heat Deposition in the Shield between the Homogeneous Model and the Heterogeneous Model (MCNP Results)

	Hetero.	Homo.	Hetero./Homo. Ratio
Total Neutron Flux (fsd)	7.47-10(0.121)	4.64-10(0.184)	1.61
Gamma Ray Flux (fsd)	2.03-10(0.219)	3.00-10(0.244)	0.677
Neutron Heat Deposition	4.87	4.12	1.18
SS316	2.17		
H_2O	2.71		
Gamma Ray Heat Deposition	14.99	16.48	0.910
SS316	14.36		
H_2O	0.63		
Total Heat Deposition	19.86	20.6	0.964

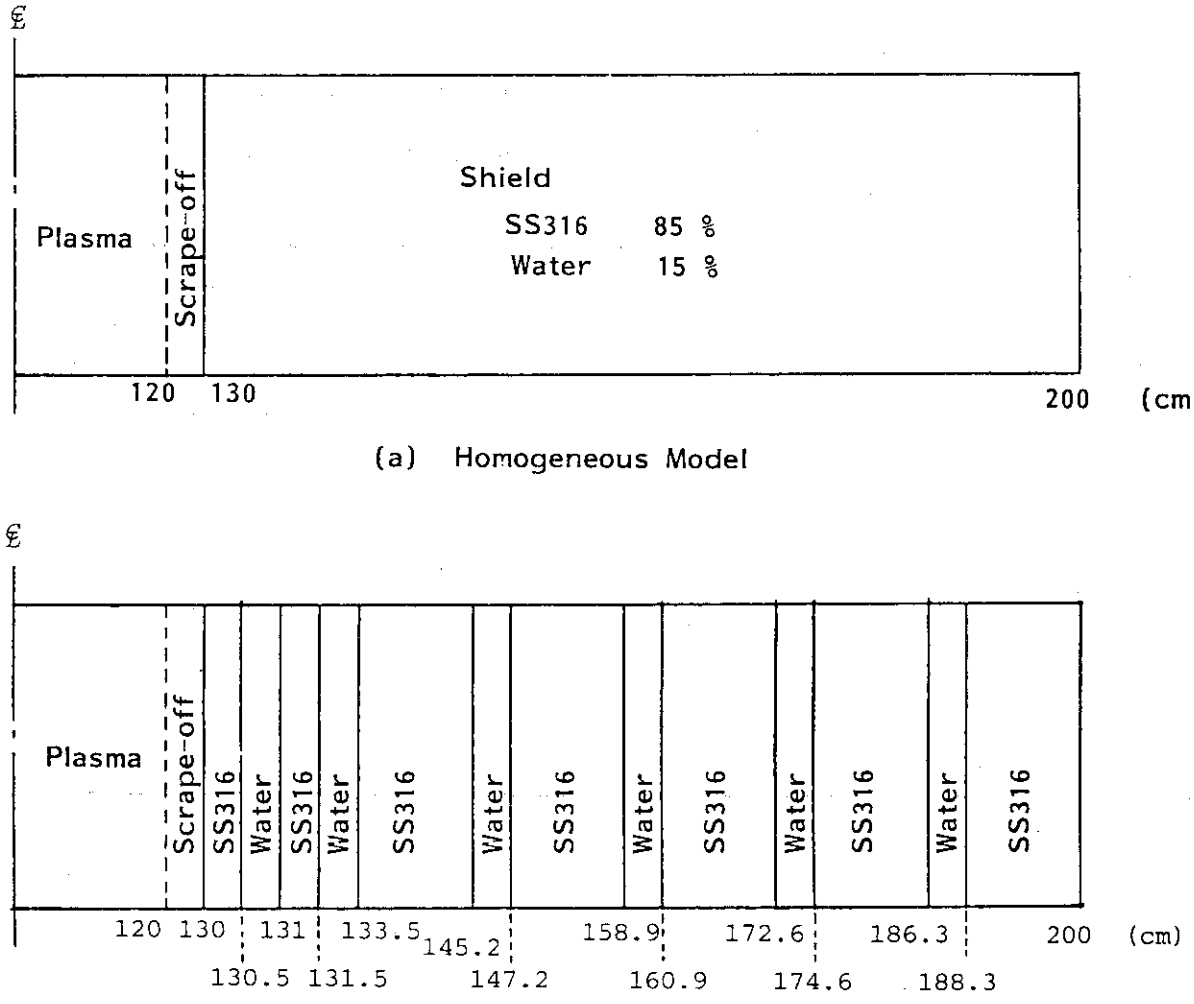

Fig. 4.1 One-Dimensional Cylindrical Models: (a) Homogeneous Model, (b) Heterogeneous Model

5. Concluding Remarks

Required accuracy of the shielding properties is around a factor of 2 at a superconducting magnet behind about 70 cm thick shield. The calculated values agrees with each other with discrepancies below a factor of 2 if relatively new data are used, as shown in the chapter 3. Regarding to the comparison with the experimental data, the E/C ratio is about 2 for the much thinner system than the actual reactor shield even if the currently most accurate method (i.e. continuous energy Monte Carlo) is used. If this E/C ratio is taken into account, though this experiment is not for the actual shield configuration, uncertainty of the current calculation will be much more than a factor of 4, and it is too large compared with the required accuracy.

Another important point to be stressed is the need for an improvement of calculation of nuclear heat deposition. This includes the improvement of the secondary gamma ray production cross section and neutron and gamma kerma factors. Energy balance must be examined in generating cross section library.

Further R&D issues are summarized as follows;

(1) Shielding benchmark experiment
- Actual shield configuration --- SS316, tungsten, water, etc.
- Thickness --- 50 - 100 cm
- Measurement --- Neutron (incl. low energy) and gamma ray
- To define E/C ratio

(2) To revise cross section library for shielding design
- Neutron and gamma ray coupled library with kerma factors
- Number of groups --- the same as GICX40
- Weighting function --- to be investigated
- Nuclear data file --- e.g. JENDL-3

(3) Sensitivity analysis
- To clear important material and reaction type for each shielding responses of superconducting magnet (e.g. copper dpa, nuclear heat deposition)
- To assess the current uncertainty level of each cross section data to be used in shield design

(4) To further investigate the effect of geometrical representation of the shield

Acknowledgement

Authors gratefully acknowledge the valuable assistance from Drs. H. Iida, S. Matsuda, S. Tamura, and M. Yoshikawa. They also would like to thank Drs. K. Kosako and K. Sakurai for supplying FSXJ3T1 and MCNP library based on JENDL-3T, and the members of the FER design team for their helpful advice and comments to this analytical work.

References

(1) M.A. Abdou, J. Nucl. Mater., 72 (1978) 147
(2) T. Kobayashi et. al., JAERI-M 87-139 (in Japanese) (1987)
(3) R.G. Alsmiller, et. al., Nucl. Technol., 4 (1977) 376
(4) K. Furuta et. al., J. Nucl. Sci. Technol., 24(4) (1987) 333
(5) S. Mori et. al., JAERI-M 87-083 (in Japanese) (1987)
(6) T. Kobayashi et. al., JAERI-M 87-138 (in Japanese) (1987)
(7) W.W. Engle Jr., K-1693, Union Carbide Corp. (1967)
(8) Y. Seki and H. Iida, JAERI-M 8818 (1980)
(9) M.K. Drake (edited), BNL-50274, ENDF 102, vol.1 (1970, revised 1974)
(10) Y. Seki et. al., private communication
(11) Y. Seki, JAERI-M 83-061 (1983)
(12) K. Kosako, private communication (1987)
(13) JENDL Compilation Group (Nuclear Data Center, JAERI): JENDL-3T, private communication (1987)
(14) R.W. Roussin et. al., ORNL-RSIC-37
(15) LASL Group TD-6, LA-7396-M, LASL (1978)
(16) M.A. Abdou and R.W. Conn, Nucl. Sci. Eng., 55 (1974) 256
(17) N.E. Hertel et. al., Fusion technol., 9 (1986) 345
(18) Y. Oka et. al., JAERI-M 87-203 (1987)

Acknowledgement

Authors gratefully acknowledge the valuable assistance from Drs. H. Iida, S. Matsuda, S. Tamura, and M. Yoshikawa. They also would like to thank Drs. K. Kosako and K. Sakurai for supplying FSXJ3T1 and MCNP library based on JENDL-3T, and the members of the FER design team for their helpful advice and comments to this analytical work.

References

(1) M.A. Abdou, J. Nucl. Mater., 72 (1978) 147
(2) T. Kobayashi et. al., JAERI-M 87-139 (in Japanese) (1987)
(3) R.G. Alsmiller, et. al., Nucl. Technol., 4 (1977) 376
(4) K. Furuta et. al., J. Nucl. Sci. Technol., 24(4) (1987) 333
(5) S. Mori et. al., JAERI-M 87-083 (in Japanese) (1987)
(6) T. Kobayashi et. al., JAERI-M 87-138 (in Japanese) (1987)
(7) W.W. Engle Jr., K-1693, Union Carbide Corp. (1967)
(8) Y. Seki and H. Iida, JAERI-M 8818 (1980)
(9) M.K. Drake (edited), BNL-50274, ENDF 102, vol.1 (1970, revised 1974)
(10) Y. Seki et. al., private communication
(11) Y. Seki, JAERI-M 83-061 (1983)
(12) K. Kosako, private communication (1987)
(13) JENDL Compilation Group (Nuclear Data Center, JAERI): JENDL-3T, private communication (1987)
(14) R.W. Roussin et. al., ORNL-RSIC-37
(15) LASL Group TD-6, LA-7396-M, LASL (1978)
(16) M.A. Abdou and R.W. Conn, Nucl. Sci. Eng., 55 (1974) 256
(17) N.E. Hertel et. al., Fusion technol., 9 (1986) 345
(18) Y. Oka et. al., JAERI-M 87-203 (1987)